

Exploring Astrophysically-Relevant Superadiabaticity Driven by Non-Resonant Heating in a Laboratory Magnetized Plasma

Ayesha Nanda* and Sudeep Bhattacharjee†

Department of Physics, Indian Institute of Technology Kanpur, Kanpur - 208016, India

(Dated: May 27, 2024)

The polytropic index of electrons in a magnetized plasma is experimentally investigated in the presence of external heating and anisotropic work done on the system by the magnetic field, incorporating the effective dimensionality in an anisotropic plasma. The measurements clearly demonstrate localized regions of superadiabatic electrons due to particle acceleration and energization through non-resonant betatron and Fermi heating processes. In regions where wave-induced heating through electron cyclotron resonance dominates, the plasma electrons behave adiabatically. The realization of superadiabaticity is universal where heating dominates the work done and has broader implications for energy exchange processes in astrophysically-relevant plasmas.

Thermodynamics has been largely explored in local thermodynamic equilibrium systems to understand the exchange of heat, energy, and work [1, 2]. The polytropic index (γ) is an important parameter that characterizes compression or expansion in a thermodynamic system and, equivalently, heat transfer processes [3]. The polytropic behavior of plasmas, both in laboratory experiments and in space, has been the subject of extensive investigation [4–7]. However, energy conversion in weakly collisional or collisionless plasmas, which is far from local thermodynamic equilibrium, is a forefront research area [8–10]. γ is equal to unity for an isothermal case, equal to infinity for an isometric case, and to the ratio of the specific heat, $\gamma_a (= 1 + 2/f$, with f kinetic degrees of freedom) for an adiabatic case. Therefore, instead of a fixed polytropic index, the theory of polytropic thermodynamic processes is extended to a superposition of polytropic indices in space and astrophysical plasmas [11].

Mostly, astrophysical plasmas have polytropic index close to the adiabatic process ($\gamma \rightarrow \gamma_a$), such as in solar wind [12, 13] and solar flares [14] and rarely with $\gamma < 1$ as in Saturnian magnetosphere [15] and inner heliosheath [16]. In several cases, space plasmas are also characterized by subadiabatic ($1 < \gamma < \gamma_a$) or superadiabatic ($\gamma_a < \gamma < \infty$) values; for example, subadiabaticity has been observed in coronal mass ejections [17, 18], solar corona [19], Earth’s plasma sheet [20, 21], planetary atmospheres [15], galaxy clusters and superclusters [22, 23],

and superadiabaticity in planetary bow shocks [24, 25]. Recently, few space plasmas [26] such as Alfvénic solar wind [4], turbulence compressed solar wind near the sun [27] have reported superadiabatic polytropic index observed during high plasma compression and high speed stream interaction [29]. $\gamma > 1$ occurs when density compressions are associated with plasma heating, whereas $\gamma < 1$ means plasma heating with density rarefactions [5]. The pictorial illustration of the polytropic index spectrum as per current understanding is shown in Fig. 1.

In laboratory, the experiments conducted under adiabatic conditions (no heating source) have shown an isothermal polytropic index [30], corroborating solar wind expansion during propagation in interplanetary space [31–33]. This approaching isothermal behavior has been a subject of extensive investigation under different conditions, such as plasmas with both Maxwellian [6] and non-Maxwellian electron energy probability functions (EEPF) [34], the latter portraying a strong dependence on the shape of EEPF due to non-local effects introduced by current-free double layers [35] and sheath electric fields [36]. Further, the electrons with energies higher than the space potential exhibit adiabatic behavior [7, 37], which indicates that the magnetic field can behave as an adiabatic wall with no physical boundary [7, 37, 38]. In all the aforementioned works, the polytropic index is calculated using kinetic degrees of freedom (f) lies in the subadiabatic region, yielding either isothermal or adiabatic indices [7, 37–40]. However, an accurate description of the attainment of superadiabaticity remains a challenge due to the complex heating mechanisms and rapidly evolving plasma dynamics, and to the best of our knowledge has neither been observed in the laboratory nor investigated in detail in space.

In this Letter, we report for the first time the experimental observation of superadiabatic electrons in a magnetized laboratory plasma in the presence of external heating and anisotropic work done on the system by the magnetic field along various directions, incorporating effective dimensionality ($\neq f$) [28]. Unique to the present study is the local obtainment of superadiabatic

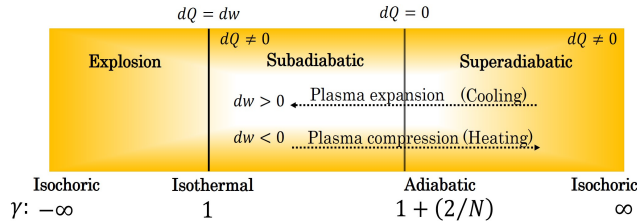


FIG. 1. Illustration of the polytropic index spectrum: dQ is the heat applied and dw is the work done.

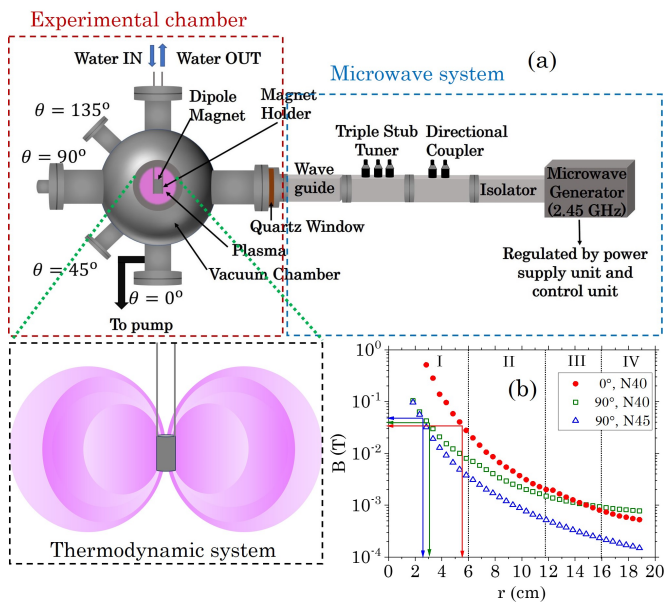


FIG. 2. (a) Schematic of the experimental set-up consisting of the experimental chamber and microwave system. Plasma is confined by a dipole magnet inside the experimental chamber, which is the thermodynamic system for the present study. (b) Measured magnetic field strength with radial distance in the polar (closed symbol) and equatorial (open symbol) regions of NdFeB cylindrical magnets of grade N40 (length 4.1 cm) and N45 (length 1.8 cm), both having a diameter of 2.3 cm, using a Lakeshore 421 gaussmeter. Solid lines corresponds to the radial location and magnetic field, where plasma frequency is equal to the electron cyclotron frequency.

polytropic indices, driven by non-resonant betatron and Fermi heating processes resulting from particle acceleration in a guiding center of a non-uniform field.

For the present study, the experiment was performed in a compact dipole plasma apparatus, as illustrated in Fig. 2(a). The plasma confined by a dipole magnetic field has been chosen for the present study due to the structural resemblance with the space plasma [41] having a distinct pattern of alternate bright and less bright regions similar to the radiation belts [42] with evidence of the phenomenon of inward diffusion [43]. The experimental set-up comprises of a spherical vacuum chamber, evacuated to a base pressure of 1 μ Torr through the combined action of a turbo molecular pump and a dry scroll pump. Argon and hydrogen plasma are used as test mediums, and the results for argon are presented. Plasma generation is achieved through electron cyclotron resonance (ECR) heating using waves of 2.45 GHz generated by a magnetron-based microwave generator. Details of the polar profile of magnetic field intensity and ECR location can be found in Ref. [44, 45]. The experiments have been performed in two sets using two different magnets: (i) N40 (length = 4.1 cm), and (ii) N45 (length = 1.8 cm) grade cylindrical magnets, both

having diameter of 2.3 cm. Their magnetic field profiles are shown in Fig. 2(b), which is non-uniform along r and at two different polar angles θ . The plasma is magnetically confined until ~ 20 cm from the center of the chamber. The confinement is notably stronger until a point ($r \sim 8$ cm), beyond which the space potential starts to decrease [43, 45]. The vertical and horizontal solid lines correspond to the radial position (in cm) and magnetic field (in T) where $\omega_p = \omega_c$, which is attained at 5.5 cm ($\theta = 0^\circ$, N40), 3.1 cm ($\theta = 90^\circ$, N40) and 2.6 cm ($\theta = 90^\circ$, N45); ω_p and ω_c being the plasma and electron cyclotron frequency respectively. In table I, the characteristic magnetic field scale length ($|B/\nabla B|$), electron Larmor radius (r_L) and ω_p/ω_c are tabulated at fixed radial distances selected from each region (separated by vertical dashed lines in Fig. 2(b)) for $\theta = 90^\circ$. The diagnostics used in this work are Langmuir probe with appropriate Bohm [45] and geometric correction [44] to the probe collection area due to the magnetized plasma, and the linear antenna for wave electric field measurements using micro-coax microwave grade RG316 (DC–3 GHz) cables with desired calibration [46]. The operating conditions are systematically controlled at the pressure of 0.4, 1.2 and 2.0 mTorr and input wave power of 300, 351 and 399 W. The construction of the diagnostics and operation details of the experimental system can be found in the works of Nanda *et al* [46, 47].

TABLE I. Magnetic field scale length, $|B/\nabla B|$ (in cm), Larmor radius, r_L (in cm) and the ratio of plasma frequency (ω_p) to electron cyclotron frequency (ω_c) at fixed radial distances from four regions – I ($r = 3$ cm), II ($r = 9$ cm), III ($r = 14$ cm) and IV ($r = 18$ cm).

r (in cm)	$ B/\nabla B $ (in cm)		r_L (in cm)		ω_p/ω_c	
	N40	N45	N40	N45	N40	N45
3	1.26	0.87	0.02	0.03	0.86	2.00
9	3.57	2.78	0.20	0.39	20.21	39.06
14	8.73	4.62	0.38	1.07	37.04	107.78
18	19.85	7.43	0.49	1.59	43.37	179.96

The polytropic index in the presence of external heat applied to the system can be obtained as [4, 28],

$$\gamma_{\perp \text{ or } \parallel} = 1 + (\gamma_a^* - 1) \left[1 - \left(\frac{dQ}{dw} \right)_{\perp \text{ or } \parallel} \right], \quad (1)$$

where dQ is the heat supplied to the system, dw is the work done by (or on) the system having positive (or negative) values signifying plasma expansion (or compression) and γ_a^* ($= 1 + (2/f^*)$) is the modified adiabatic index in an anisotropic plasma, f^* being the effective dimensionality, which depends on kinetic degrees of freedom f and

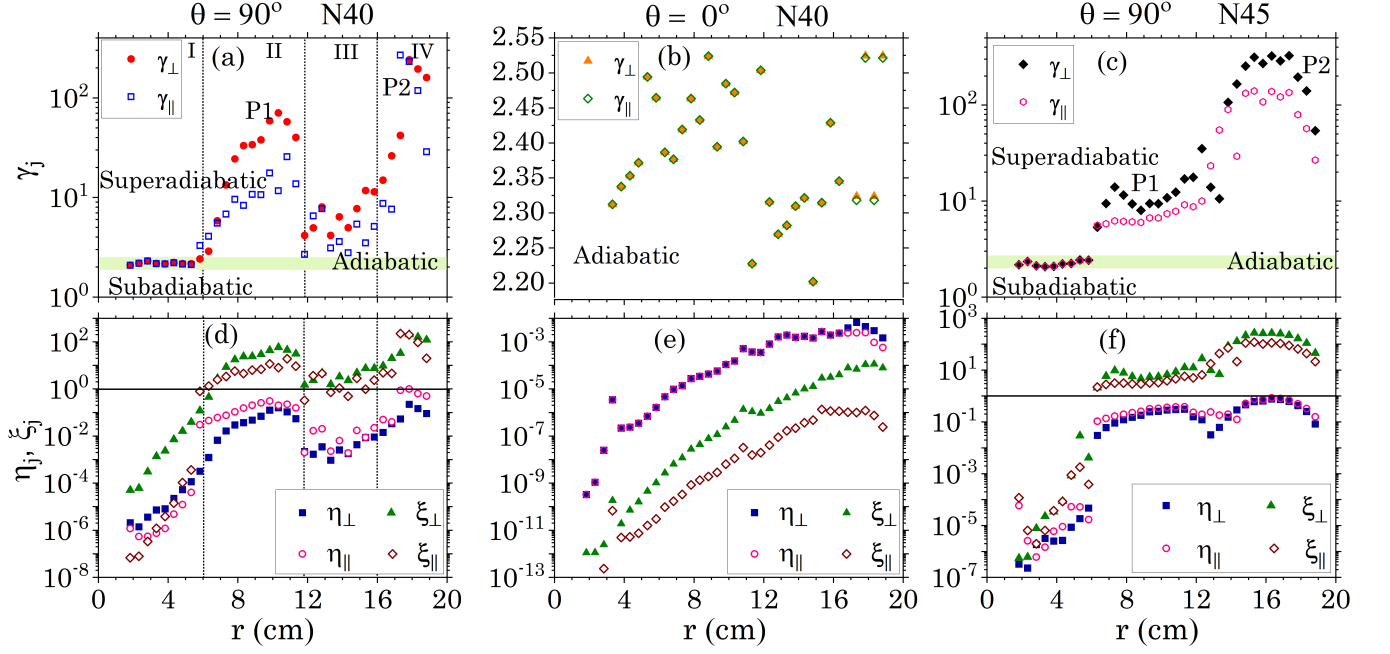


FIG. 3. Radial profiles of [(a)–(c)] γ_j (top panel) and [(d)–(f)] η_j and ξ_j (bottom panel) for $j \rightarrow \perp, \parallel$ in the equatorial ($\theta = 90^\circ$) [(a),(d)] and polar ($\theta = 0^\circ$) plane [(b),(e)] with N40 grade magnet, and in the equatorial ($\theta = 90^\circ$) plane [(c),(f)] with N45 grade magnet. The error corresponding to the standard deviation in γ_j is within 5% and in η_j, ξ_j is within 8%. The green band represents the adiabatic regions in (a) and (c).

anisotropy $\alpha (= T_{e\perp}/T_{e\parallel})$, given by [28],

$$f^* = \frac{1 + (f - 1)^2 \alpha^2}{1 + (f - 1) \alpha^2}, \quad (2)$$

and holds good for $\alpha < 2$ [28]. In our experiments, α lies between 0.7–1.7 [47]. Furthermore, in an anisotropic fluid, the magnetic field-associated terms exchange parallel and perpendicular energy, and they provide additional work. The perpendicular and parallel work in the presence of magnetic field (B) are given by [49, 50],

$$dw_{\perp} = -p_{\perp} V d(\ln B) \quad \text{and} \quad dw_{\parallel} = -p_{\parallel} V d\left(\ln \frac{N_e}{B}\right), \quad (3)$$

respectively, with N_e and V being the electron density and local plasma volume. The perpendicular and parallel polytropic indices can be derived as,

$$\gamma_{\perp} = 1 + (\gamma_a^* - 1) \left[1 + \left(\underbrace{\frac{1}{k_B T_{e\perp} v_{\perp} \nabla_{\perp} (\ln B)}}_{\eta_{\perp}} + \underbrace{\frac{1}{k_B T_{e\perp} v_{\perp} \nabla_{\perp} (\ln B)}}_{\xi_{\perp}} \right) \right], \quad (4)$$

$$\gamma_{\parallel} = 1 + (\gamma_a^* - 1) \left[1 + \left(\underbrace{\frac{1}{k_B T_{e\parallel} v_{\parallel} \nabla_{\parallel} \ln(N_e/B)}}_{\eta_{\parallel}} + \underbrace{\frac{1}{k_B T_{e\parallel} v_{\parallel} \nabla_{\parallel} \ln(N_e/B)}}_{\xi_{\parallel}} \right) \right]. \quad (5)$$

Here, k_B is the Boltzmann constant, $T_{e\perp}$ and $T_{e\parallel}$ are the electron temperatures, v_{\perp} and v_{\parallel} are the fluid velocities obtained by solving the momentum equation [47], and $W_{M\perp}$ and $W_{M\parallel}$ represents the direct wave-induced heating dependent on its local electric field intensity; from henceforth referred to as wave-induced heating, given by [51, 52],

$$W_{Mj} = \frac{e E_{1j}^2}{m_e} \frac{\nu_{hj}}{\nu_{hj}^2 + (\omega - \omega_{cj})^2}, \quad (6)$$

where, E_{1j} is the wave electric field, ν_{hj} is the electron-neutral collision frequency, ω_{cj} is the electron cyclotron frequency for $j \rightarrow \perp, \parallel$, ω is the angular wave frequency, e and m_e are the electronic charge and mass. The effective plasma parameters used in the present work are calculated by integrating over the EEPFs [37, 39], obtained by the Druyvesteyn technique [53]. The analysis holds good for regions with $r_L > r_p$, $r_p (= 4 \text{ mm})$ being the probe tip radius. For regions with $r_L < r_p$, Bohm correction is employed to correct the electron current measured by the Langmuir probe. This correction adapts the

Langmuir probe theory for unmagnetized plasma to be validated for magnetized plasmas [45]. Apart from the wave-induced heating (cf. Eq. 6) along the perpendicular and parallel directions, in a guiding center approximation, two acceleration processes contribute to the kinetic energy density of electrons: Fermi acceleration due to the particle motion along the curved field lines in high \mathbf{B} -curvature regions [54, 55] and betatron acceleration associated with the conservation of magnetic moment [56] in regions of strong \mathbf{B} -gradients [57]. In our case, $r_L < |B/\nabla B|$ (cf. Table I), and electrons gyrating will experience curvatures in their trajectories as they traverse through varying magnetic (∇B) field through the Lorentz force. Moreover, the electrons satisfy the guiding centre approximation only when the curvature parameter, $\kappa = \sqrt{R_c/r_L} > 3$ [58], where $R_c [=(\hat{B} \cdot \nabla)\hat{B}]^{-1}$ is the curvature radius. Experimentally, κ lies between 5–120, implying its applicability. Betatron acceleration increases the perpendicular energy of an electron, whereas Fermi acceleration enhances electron energy in the field-aligned direction [59], and the heating rates for a plasma at steady-state are given by [54–57, 59],

$$W_{B\perp} = \frac{T_{e\perp}}{B} (\vec{v}_E \cdot \nabla B), \quad (7)$$

$$W_{F\parallel} = \left(T_{e\parallel} + \frac{m_e}{e} v_{\parallel}^2 \right) \vec{v}_E \cdot (\hat{B} \cdot \nabla \hat{B}), \quad (8)$$

where \hat{B} is the magnetic field unit vector and \vec{v}_E is the $\vec{E} \times \vec{B}$ drift velocity arising from the total electric field $\vec{E}(\vec{r}, t) = \vec{E}_0(\vec{r}) + \vec{E}_1(\vec{r}, t)$, where $\vec{E}_0(\vec{r})$ is the electrostatic field resulting from the gradient of the space potential and $\vec{E}_1(\vec{r}, t)$ is the wave electric field [46]. In the present experiment, $\vec{E} \cong \vec{E}_1$ since $|\vec{E}_0| \ll |\vec{E}_1|$, and the drift velocity is primarily governed by \vec{E}_1 . However, situation may arise where $\vec{E} \cong \vec{E}_0$ when \vec{E}_1 is either absent or weak in comparison to \vec{E}_0 . Thus, $W_{B\perp}$ and $W_{F\parallel}$ arise from the effect of particle drift velocities due to the local electric and magnetic field.

Radial profiles of γ_j in the presence of external heat in the equatorial ($\theta = 90^\circ$) and polar ($\theta = 0^\circ$) regions using Eq. 4 and 5 are plotted in Fig. 3(a)–3(c). In Fig. 3(a) the polytropic index is nearly adiabatic ($\gamma_j \rightarrow \gamma_a^*$ and $\gamma_a^* = 1 + (2(1 + 2\alpha^2)/(1 + 4\alpha^2))$) for electrons with three degrees of freedom (cf. Eq. 2)) in region I, approaches adiabatic value in region III and superadiabatic ($\gamma_j > \gamma_a^*$) values in region II and IV in the equatorial plane. However, the adiabatic limit is maintained in the overall polar region (cf. Fig. 3(b)), which appears to be at odds with that obtained in the equatorial plane ($\theta = 90^\circ$) (cf. Fig. 3(a)) exhibiting superadiabaticity in distinct localized regions. Furthermore, in the equatorial region, with N45 grade magnet having slightly lower magnetic field (characterized by relatively smaller r_L and $|B/\nabla B|$

(cf. Table I)), electrons behave superadiabatically for $r > 6$ cm.

To further understand the superadiabatic nature, radial profiles of the ratio of wave-induced heating to the work done ($\eta_{\perp\text{or}\parallel}$) and Betatron (or Fermi) heating to the work done ($\xi_{\perp\text{or}\parallel}$) (cf. Eq. 4 and 5), are plotted in Fig. 3(d)–3(f) at the same locations and operating conditions, as in Fig. 3(a)–3(c). The work done by the electrons along perpendicular and parallel directions is negative (cf. Eq. 3), and negative work implicates a plasma compression due to trapping of electrons in the magnetic field lines, forbidding plasma cooling by expansion. The positive heat supplied to the system (cf. Eq. 6, 7 and 8) and negative work (cf. Eq. 3) indicates that the system is simultaneously receiving energy from two different sources – heat and work, resulting in increase in the internal energy of the system. Moreover, it is clearly observed that in the equatorial plane $\eta_j < \xi_j$ (cf. Fig. 3(d) and 3(f)), whereas in the polar region $\eta_j > \xi_j$ (cf. Fig. 3(e)), and hence betatron and Fermi heating, and wave-induced heating regulates the γ_j values at $\theta = 90^\circ$ and $\theta = 0^\circ$ respectively. In the equatorial region, near the magnet ($r < 6$ cm) $\xi_j \ll 1$ and $\gamma_j \rightarrow \gamma_a^*$, and in regions at and beyond $r = 6$ cm $\xi_j \geq 1$ resulting in $\gamma_j > \gamma_a^*$ (cf. Fig. 3(a), 3(c), 3(d) and 3(f)). However, at $\theta = 0^\circ$, $\eta_j \ll 1$ and $\gamma_j \rightarrow \gamma_a^*$ (cf. Fig. 3(b) and 3(e)).

Besides, the physics of the work done by the magnetic field lines can be explained as follows. At $\theta = 90^\circ$, near the magnet ($r < 6$ cm), stronger magnetic field (low ω_p/ω_c value as in Table I) acts as a pseudo wall doing more work on the system in comparison to any heating (betatron, Fermi, or wave-induced), but as it is not a physical boundary, so no heat is transferred [7], resulting in nearly adiabatic plasma. In other regions, the efficiency of the work done by the magnetic field decreases (ω_p/ω_c increases rapidly away from the magnet), and betatron (along perpendicular direction) and Fermi (along parallel direction) heating control the polytropic nature of plasma.

To assess the relevance of various types of heating with the superadiabatic behavior of electrons, radial profiles of the rate of betatron ($W_{B\perp}$), Fermi ($W_{F\parallel}$) and wave-induced (W_{Mj}) heating are shown in Fig. 4 for $\theta = 0^\circ$ and 90° . Heating rates due to betatron and Fermi acceleration peak at the regions where the polytropic index exhibits deviation from the adiabatic index with hot electron populations, indicating local efficient heating contributing to the total energy of the system. $W_{B\perp}$ and $W_{F\parallel}$ in the polar region increases towards the weaker field region and peaks at $r \sim 15 - 18$ cm (cf. Fig. 4(a)), whereas $W_{B\perp}$ and $W_{F\parallel}$ in the equatorial region peaks in unison between 6–12 cm and 16–18 cm (cf. Fig. 4(c)) using N40 grade magnet and with two consecutive peaks beyond $r > 6$ cm (cf. Fig. 4(e)) using N45 grade magnet (having weaker magnetic field strength than N40 grade magnet (cf. Fig. 2(b))). In the polar region (cf. Fig.

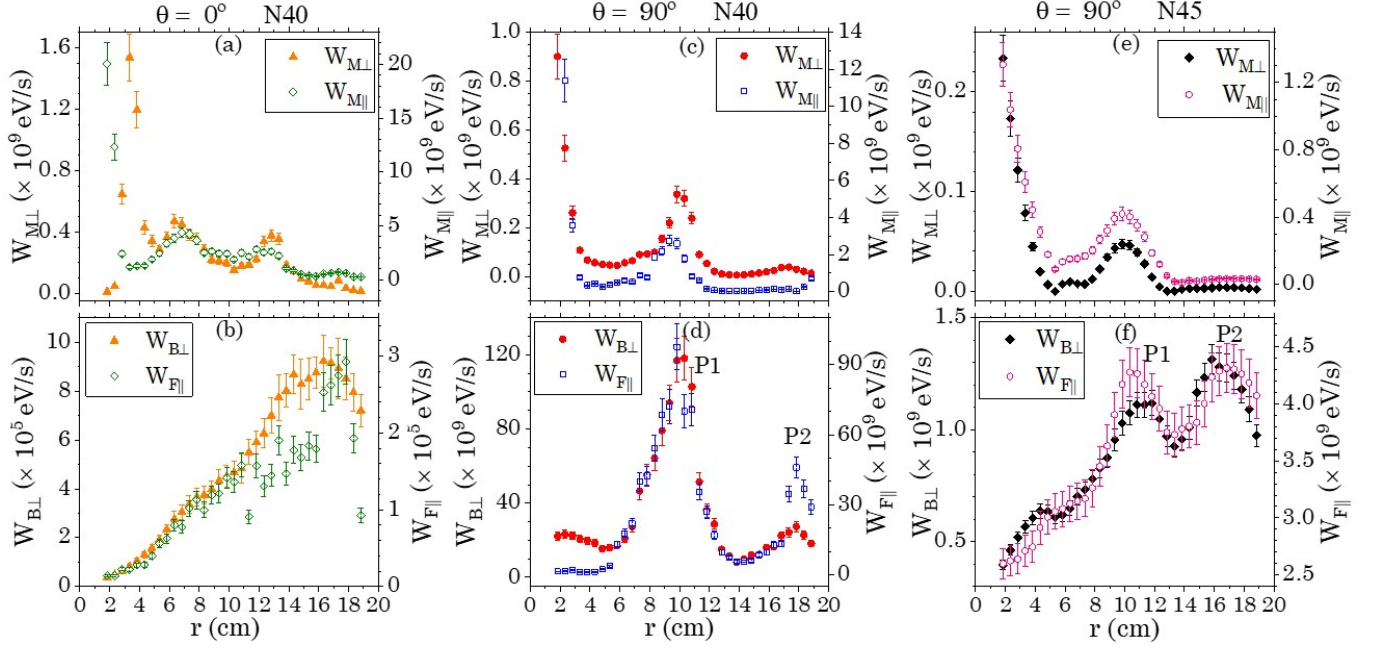


FIG. 4. Radial profiles of heating rates for $\theta = 0^\circ$ [(a)–(b)], $\theta = 90^\circ$ [(c)–(d)] with N40 grade magnet and $\theta = 90^\circ$ [(e)–(f)] with N45 grade magnet. Top panel: betatron, $W_{B\perp}$ (left y-axis) and Fermi, $W_{F\parallel}$ (right y-axis) heating rates, bottom panel: perpendicular (left y-axis) and parallel (right y-axis) wave-induced heating rates, at 1.2 mTorr pressure and 300 W wave power.

4(a) and 4(b)), $W_{M\perp}$ exceeds $W_{B\perp}$ by $\sim 10^2 - 10^4$ (left y-axis), and $W_{M\parallel}$ exceeds $W_{F\parallel}$ by $\sim 10^3 - 10^6$ (right y-axis). This means that the polar region is dominated by wave-induced heating and is found to have polytropic index close to the adiabatic process ($\gamma_j \rightarrow \gamma_a^*$). Furthermore, in the equatorial plane, $W_{B\perp}/W_{M\perp} \sim 10^2$ in P1 and P2, and $W_{F\parallel}/W_{M\parallel} \sim 10$ in P1 and P2 for N40 grade magnet, and for N45 grade magnet both $W_{B\perp}/W_{M\perp}$ and $W_{F\parallel}/W_{M\parallel}$ are ~ 10 in P1 and $\sim 10^2$ in P2. This indicates in the equatorial plane $W_{B\perp}$ and $W_{F\parallel}$ regulate superadiabaticity along the perpendicular and parallel directions respectively, and calls for the existence of a threshold heating for the attainment of superadiabaticity. From the observations, it can be concluded that the superadiabaticity is an outcome of the governance of betatron and Fermi heating with peaks at same radial locations (cf. Fig. 4(c) and Fig. 3(a), and Fig. 4(e) and Fig. 3(c)). It has been verified that a similar correlation between the superadiabatic nature of plasma associated with various heating processes and the anisotropic work done is also observed in hydrogen plasma, but at different radial locations ($r > 9$ cm) and is not shown here. In regions where wave-induced heating through electron cyclotron resonance dominates, the plasma electrons behave adiabatically ($\gamma_j \rightarrow \gamma_a^*$).

In conclusion, this Letter investigates the effect of heating on the thermodynamics of electrons in the presence of an electric field and the work done by the magnetic field, considering the effective dimensionality in an anisotropic plasma. The experiment demonstrates local regions in

weaker field regime with superadiabatic electrons for the first time in a laboratory magnetized plasma. Results indicate that the local superadiabatic electrons are due to heating through betatron and Fermi acceleration along perpendicular and parallel directions, respectively. The macroscopic study of the polytropic behavior enables us to enhance our understanding of the heating mechanisms in the energy exchange processes. The specific behavior of energy exchange in a superadiabatic system can vary widely based on the nature of the energy sources, associated particle drift velocities, the thermodynamical processes involved, and the system's characteristics (the magnetic field confinement, independent of the chamber shape and size). Therefore, the investigation of power balance along with the interactions within the system is necessary for gaining insight into the intricate dynamics of heat and work in superadiabatic regions, and will be taken up in the future.

The authors express their gratitude to the funding agency Council of Scientific and Industrial Research (CSIR), India, through Grant No. 03/1496/23/EMR-II. Ayesha Nanda gratefully acknowledges doctoral fellowship under the INSPIRE programme (IF180114) of Department of Science & Technology (DST), India.

* ayesha@iitk.ac.in

† sudeepb@iitk.ac.in

- [1] Y. A. Cengel, M. A. Boles, and M. Kanoğlu, *Thermodynamics: an engineering approach*, Vol. 5 (McGraw-hill New York, 2011).
- [2] D. Jou, J. Casas-Vázquez, G. Lebon, D. Jou, J. Casas-Vázquez, and G. Lebon, *Extended irreversible thermodynamics* (Springer, 1996).
- [3] M. A. Dayeh and G. Livadiotis, Polytropic behavior in the structures of interplanetary coronal mass ejections, *The Astrophysical Journal Letters* **941**, L26 (2022).
- [4] Z. I. Shaikh, A. N. Raghav, G. Vichare, R. D’Amicis, and D. Telloni, Evidence for superadiabatic heating and cooling of alfvénic solar wind, *Monthly Notices of the Royal Astronomical Society: Letters* **519**, L62 (2023).
- [5] K. Stasiewicz, Ion-pressure equations derived from measurements in space, *Physical Review Letters* **95**, 015004 (2005).
- [6] J. Little and E. Choueiri, Electron cooling in a magnetically expanding plasma, *Physical Review Letters* **117**, 225003 (2016).
- [7] K. Takahashi, C. Charles, R. Boswell, and A. Ando, Adiabatic expansion of electron gas in a magnetic nozzle, *Physical Review Letters* **120**, 045001 (2018).
- [8] P. A. Cassak, M. H. Barbhuiya, H. Liang, and M. R. Argall, Quantifying energy conversion in higher-order phase space density moments in plasmas, *Physical Review Letters* **130**, 085201 (2023).
- [9] G. G. Howes, A prospectus on kinetic heliophysics, *Physics of plasmas* **24** (2017).
- [10] W. H. Matthaeus, Y. Yang, M. Wan, T. N. Parashar, R. Bandyopadhyay, A. Chasapis, O. Pezzi, and F. Valentini, Pathways to dissipation in weakly collisional plasmas, *The Astrophysical Journal* **891**, 101 (2020).
- [11] G. Livadiotis, Superposition of polytropes in the inner heliosheath, *The Astrophysical Journal Supplement Series* **223**, 13 (2016).
- [12] G. Nicolaou, G. Livadiotis, and X. Moussas, Long-term variability of the polytropic index of solar wind protons at 1 au, *Solar Physics* **289**, 1371 (2014).
- [13] G. Livadiotis and M. Desai, Plasma-field coupling at small length scales in solar wind near 1 au, *The Astrophysical Journal* **829**, 88 (2016).
- [14] T. Wang, L. Ofman, X. Sun, E. Provornikova, and J. M. Davila, Evidence of thermal conduction suppression in a solar flaring loop by coronal seismology of slow-mode waves, *The Astrophysical Journal Letters* **811**, L13 (2015).
- [15] K. Dialynas, E. Roussos, L. Regoli, C. P. Paranicas, S. M. Krimigis, M. Kane, D. G. Mitchell, D. C. Hamilton, N. Krupp, and J. F. Carbary, Energetic ion moments and polytropic index in saturn’s magnetosphere using cassini/mimi measurements: A simple model based on κ -distribution functions, *Journal of Geophysical Research: Space Physics* **123**, 8066 (2018).
- [16] G. Livadiotis and D. McComas, Understanding kappa distributions: A toolbox for space science and astrophysics, *Space Science Reviews* **175**, 183 (2013).
- [17] W. Mishra and Y. Wang, Modeling the thermodynamic evolution of coronal mass ejections using their kinematics, *The Astrophysical Journal* **865**, 50 (2018).
- [18] Y. Liu, J. Richardson, J. Belcher, J. Kasper, and H. Elliott, Thermodynamic structure of collision-dominated expanding plasma: Heating of interplanetary coronal mass ejections, *Journal of Geophysical Research: Space Physics* **111** (2006).
- [19] S. K. Prasad, J. Raes, T. Van Doorselaere, N. Magyar, and D. Jess, The polytropic index of solar coronal plasma in sunspot fan loops and its temperature dependence, *The Astrophysical Journal* **868**, 149 (2018).
- [20] X. Zhu, Plasma sheet polytropic index as inferred from the fpe measurements, *Geophysical Research Letters* **17**, 2321 (1990).
- [21] C. Goertz and W. Baumjohann, On the thermodynamics of the plasma sheet, *Journal of Geophysical Research: Space Physics* **96**, 20991 (1991).
- [22] S. De Grandi and S. Molendi, Temperature profiles of nearby clusters of galaxies, *The Astrophysical Journal* **567**, 163 (2002).
- [23] M. W. Bautz, E. D. Miller, J. S. Sanders, K. A. Arnaud, R. F. Mushotzky, F. S. Porter, K. Hayashida, J. P. Henry, J. P. Hughes, M. Kawaharada, *et al.*, Suzaku observations of abell 1795: Cluster emission to r 200, *Publications of the Astronomical Society of Japan* **61**, 1117 (2009).
- [24] M. Tatralay, C. Russell, J. Luhmann, A. Barnes, and J. Mihalov, On the proper mach number and ratio of specific heats for modeling the venus bow shock, *Journal of Geophysical Research: Space Physics* **89**, 7381 (1984).
- [25] H. Zhuang and C. Russell, An analytic treatment of the structure of the bow shock and magnetosheath, *Journal of Geophysical Research: Space Physics* **86**, 2191 (1981).
- [26] G. Livadiotis, On the origin of polytropic behavior in space and astrophysical plasmas, *The Astrophysical Journal* **874**, 10 (2019).
- [27] G. Nicolaou, G. Livadiotis, R. T. Wicks, D. Verscharen, and B. A. Maruca, Polytropic behavior of solar wind protons observed by parker solar probe, *The Astrophysical Journal* **901**, 26 (2020).
- [28] G. Livadiotis and G. Nicolaou, Relationship between polytropic index and temperature anisotropy in space plasmas, *The Astrophysical Journal* **909**, 127 (2021).
- [29] K. Ghag, A. Raghav, Z. Shaikh, G. Nicolaou, O. Dhamane, and U. Panchal, Distinct polytropic behavior of plasma during icme-hss interaction, *arXiv preprint arXiv:2210.04065* (2022).
- [30] J. Sheehan, B. Longmier, E. Bering, C. Olsen, J. Squire, M. Ballenger, M. Carter, L. Cassady, F. C. Díaz, T. Glover, and A. V. Ilin, Temperature gradients due to adiabatic plasma expansion in a magnetic nozzle, *Plasma Sources Science and Technology* **23**, 045014 (2014).
- [31] M. Pudovkin, C.-V. Meister, and B. Besser, Adiabatic indices in a convecting anisotropic plasma, *Astronomische Nachrichten: News in Astronomy and Astrophysics* **320**, 87 (1999).
- [32] A. Retinò, A journey through scales, *Nature Physics* **12**, 1092 (2016).
- [33] T. Van Doorselaere, N. Wardle, G. Del Zanna, K. Jansari, E. Verwichte, and V. M. Nakariakov, The first measurement of the adiabatic index in the solar corona using time-dependent spectroscopy of hinode/eis observations, *The Astrophysical Journal Letters* **727**, L32 (2011).
- [34] Y. Zhang, C. Charles, and R. Boswell, Thermodynamic study on plasma expansion along a divergent magnetic field, *Physical Review Letters* **116**, 025001 (2016).
- [35] K. Takahashi, C. Charles, R. Boswell, T. Kaneko, and R. Hatakeyama, Measurement of the energy distribution of trapped and free electrons in a current-free double layer, *Physics of Plasmas* **14**, 114503 (2007).

- [36] R. W. Boswell, K. Takahashi, C. Charles, and I. D. Kaganovich, Non-local electron energy probability function in a plasma expanding along a magnetic nozzle, *Frontiers in Physics* **3**, 14 (2015).
- [37] J. Y. Kim, K. Chung, S. Kim, J. H. Ryu, K.-J. Chung, and Y. Hwang, Thermodynamics of a magnetically expanding plasma with isothermally behaving confined electrons, *New Journal of Physics* **20**, 063033 (2018).
- [38] K. Takahashi, Helicon-type radiofrequency plasma thrusters and magnetic plasma nozzles, *Reviews of Modern Plasma Physics* **3**, 3 (2019).
- [39] K. Takahashi, C. Charles, R. W. Boswell, and A. Ando, Thermodynamic analogy for electrons interacting with a magnetic nozzle, *Physical Review Letters* **125**, 165001 (2020).
- [40] Y. Zhang, C. Charles, and R. Boswell, A polytropic model for space and laboratory plasmas described by bi-maxwellian electron distributions, *The Astrophysical Journal* **829**, 10 (2016).
- [41] A. R. Baitha, A. Kumar, and S. Bhattacharjee, A table top experiment to investigate production and properties of a plasma confined by a dipole magnet, *Review of Scientific Instruments* **89**, 023503 (2018).
- [42] S. Bhattacharjee, A. R. Baitha, J. V. Mathew, and S. Bhattacharjee, Characterizing spatially varying optical emissions in a steady-state dipole plasma: inversion based experiments and modeling, *Physica Scripta* **96**, 035605 (2021).
- [43] A. R. Baitha, A. Nanda, S. Hunjan, and S. Bhattacharjee, Steady state densities in a plasma confined by a dipole magnet: Diffusion induced transport explored through direct measurements and modeling, *AIP Advances* **10**, 045328 (2020).
- [44] A. R. Baitha, A. Nanda, S. Hunjan, and S. Bhattacharjee, Particle balance in a steady state plasma in a dipole magnetic field, *Plasma Research Express* **1**, 045005 (2019).
- [45] S. Bhattacharjee, A. R. Baitha, A. Nanda, S. Hunjan, and S. Bhattacharjee, Physics of plasmas confined by a dipole magnet: insights from compact experiments driven at steady state, *Reviews of Modern Plasma Physics* **6**, 16 (2022).
- [46] A. Nanda and S. Bhattacharjee, Current density profiles in a compact dipole plasma, *Physics of Plasmas* **30**, 052107 (2023).
- [47] A. Nanda and S. Bhattacharjee, Temperature anisotropy governed electrical conductivity tensor in a steady state dipole plasma: Spatially resolved experiments and modeling, *Physics of Plasmas* **29**, 062105 (2022).
- [48] G. Livadiotis, Connection of turbulence with polytropic index in the solar wind proton plasma, *Entropy* **21**, 1041 (2019).
- [49] S. Du, G. P. Zank, X. Li, and F. Guo, Energy dissipation and entropy in collisionless plasma, *Physical Review E* **101**, 033208 (2020).
- [50] X. Guo, L. Sironi, and R. Narayan, Electron heating in low-mach-number perpendicular shocks. I. Heating mechanism, *The Astrophysical Journal* **851**, 134 (2017).
- [51] S. Bhattacharjee, H. Amemiya, and Y. Yano, Plasma buildup by short-pulse high-power microwaves, *Journal of Applied Physics* **89**, 3573 (2001).
- [52] S. Bhattacharjee, I. Dey, A. Sen, and H. Amemiya, Quasisteady state interpulse plasmas, *Journal of applied physics* **101** (2007).
- [53] A. Heiler, R. Friedl, and U. Fantz, Application of a langmuir probe ac technique for reliable access to the low energy range of electron energy distribution functions in low pressure plasmas, *Journal of Applied Physics* **127**, 113302 (2020).
- [54] J. Drake, M. Swisdak, H. Che, and M. Shay, Electron acceleration from contracting magnetic islands during reconnection, *Nature* **443**, 553 (2006).
- [55] F. Guo, H. Li, W. Daughton, and Y.-H. Liu, Formation of hard power laws in the energetic particle spectra resulting from relativistic magnetic reconnection, *Physical Review Letters* **113**, 155005 (2014).
- [56] E. Eriksson, A. Vaivads, L. Alm, D. B. Graham, Y. V. Khotyaintsev, and M. André, Electron acceleration in a magnetotail reconnection outflow region using magnetospheric multiscale data, *Geophysical Research Letters* **47**, e2019GL085080 (2020).
- [57] P. Shi, E. E. Scime, M. H. Barbhuiya, P. A. Cassak, S. Adhikari, M. Swisdak, and J. E. Stawarz, Using direct laboratory measurements of electron temperature anisotropy to identify the heating mechanism in electron-only guide field magnetic reconnection, *Physical Review Letters* **131**, 155101 (2023).
- [58] C. Shen, X. Li, M. Dunlop, Z. Liu, A. Balogh, D. Baker, M. Hapgood, and X. Wang, Analyses on the geometrical structure of magnetic field in the current sheet based on cluster measurements, *Journal of Geophysical Research: Space physics* **108** (2003).
- [59] Z. Zhong, M. Zhou, R. Tang, X. Deng, D. Turner, I. Cohen, Y. Pang, H. Man, C. Russell, B. Giles, W. Paterson, Y. Khotyaintsev, and J. Burch, Direct evidence for electron acceleration within ion-scale flux rope, *Geophysical Research Letters* **47**, e2019GL085141 (2020).